AEROSOL PROPERTIES DURING THE 2007 GLOBAL DUST STORM (MY28): SOLAR INFRARED OCCULTATION OBSERVATIONS BY SPICAM

D. S. Betsis, *(dasha-integral@yandex.ru)*, **A. A. Fedorova, O. I. Korablev**, *Space Research Institute (IKI), Moscow, Russia*, **J.-L. Bertaux, F. Montmessin**, *Service d'Aŭronomie du CNRS, Verriures-le-Buisson, France*.

Introduction:

The current analysis deals with properties of aerosol particles during the 2007 global dust storm (Mars Year 28). Such events are very important for understanding and modeling processes of the Martian climate. During this time a significant dust lifting and transport processes are observed covering the whole planet by dust haze. Atmospheric heating associated with dust absorption of solar light increases strongly making a feedback and causing high advective velocities. These effects are forcing of atmospheric circulation.

Solar occultation measurement in the IR spectral range allows to study the vertical distribution of aerosols. SPICAM on Mars-Express is a dedicated occultation experiment. It consists of ultraviolet and infrared spectrometers. Here we analyze data from the SPICAM IR (wavelengths of 1–1.7 μm) which provides information about optical properties of aerosols: opacity and extinction coefficient versus altitude.

The ratio of opacities depends primarily on the particle size distribution. Based on Mie scattering theory we can reconstruct such characteristics as effective radius and variance assuming the lognormal distribution (Montmessin et al., 2002). Both mineral dust and water ice particles interact with the solar radiation so we have used refraction index for dust (Wolff et al., 2009) and H_2O ice (Warren and Brandt, 2008).

Data set:

The IR channel of SPICAM is an infrared spectrometer employing an Acousto-Optic Tunable Filter (AOTF) and is equipped with two separate detectors, each providing a specific polarization component of the incident light (Korablev et al., 2006). The spectral resolution is nearly constant in wavenumbers and amounts to 3.5 cm^{-1}. In solar occultations, the vertical resolution depends on the spacecraft to limb distance, varying from 1000 to 13,000 km, so with the field of view 4.2 arcmin (1.2 mrad) the vertical resolution typically varies from 1 to 12 km.

We have used measurements of transmission in several spectral points outside gaseous absorption bands: such ''reference wavelengths'' are distributed in the range from 1 to 1.7 μm. The observations had a set of 11 reference wavelengths: 996.4, 1093.7, 1158.2, 1197.0, 1241.4, 1272.9, 1304.4, 1321.9, 1514.6, 1552.2 nm. A detailed description of solar occultation technique by SPICAM IR, including the issues of MARSIS antenna oscillations, light interference and the first generation retrieval algorithm is given by Fedorova et al., 2009.

Current work covers observational season Ls = 254–302° in MY28 and latitudes from 65°S to 65°N. It includes 210 useful orbits. The geographical distribution of observations is presented in Fig.1. On each point the full profile of opacity was measured up to 100 km but we selected only such altitudes which have good signal-to-noise ratio (SNR).

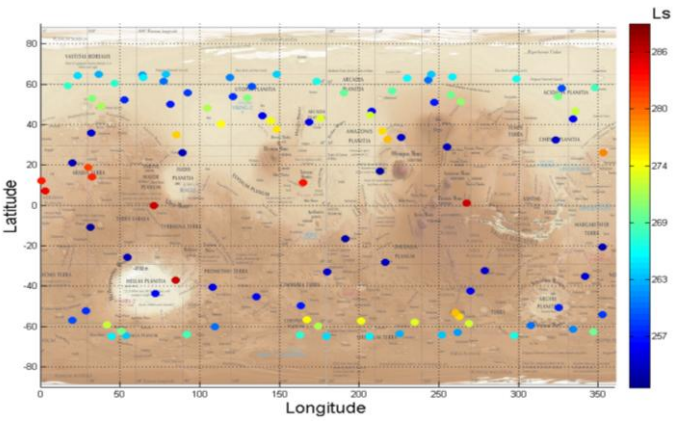

Fig. 1. The geographical distribution of observations in the perihelion season of MY28. The MOLA map (Smith et al., 1999) is used as a background for the SPICAM coverage.

Retrievals:

There are several steps of retrieval algorithm from raw data (solar radiance versus wavelengths) to particle size and number density. We can note them:

1) Correction for the dark signal taking into account a temperature drift in the instrument and signal oscillation caused by satellite attitude disturbances after deployment of MARSIS antennae.
2) Calculation of reference spectrum outside of the Martian atmosphere (above ~120 km) by combining several profiles, and calculation of slant optical depth of each layer according to Bougher–Beer–Lambert's law:
   $I_\lambda(l) = I_0 \exp(-\tau_\lambda(l))$,
   where l is the optical path in the atmosphere, I_0 is the solar flux outside the atmosphere, τ_λ is the optical depth. Pick up good points with suitable SNR.
3) Retrieval of extinction profiles using traditional "onion peeling" method at several wavelengths. The result is a value of extinction coefficient for

each level.

4) Constraining of the size particle distribution with assumption of lognormal law in a classical Mie theory. To compute light scattering by polydisperse spherical particles we applied the code by Michael Mishchenko and collaborators (Mishchenko et al., 1999). The result is parameters of distribution: the effective radius (r_{eff}) and variance (v_{eff}) for each altitude. On this step we assume 5 cases of v_{eff}: 0.1, 0.2, 0.3, 0.4 and 0.5, and 2 cases of refractive index: mineral dust and water ice. Thus, we have 10 cases of fit for each orbit.
5) Retrieval of aerosol number density using the particle size distribution and knowing the vertical profile of extinction coefficient.

We have noticed that number density values do depend on an assumption of effective variance and the SPICAM spectral range is not sensitive to the nature of particles, so we can't distinguish between dust and water ice. So we must do some additional procedures for finding the best case of fitting.

Trying to distinguish water ice clouds we can use observed cloud layers in extinction and particle sizes and use results of modeling from Martian Climate Database (MCD) which takes dust and cloud formation into account (Montabone et al., 2015) or other simultaneous in season observations.

To find the effective variances for different alti-

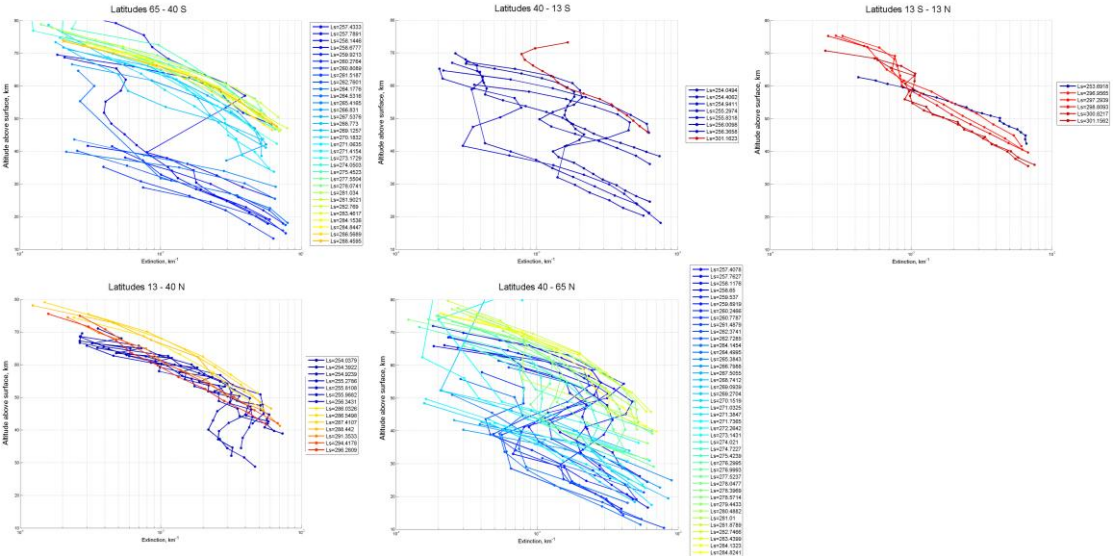

Fig. 2. Extinction profiles grouped by latitudes.

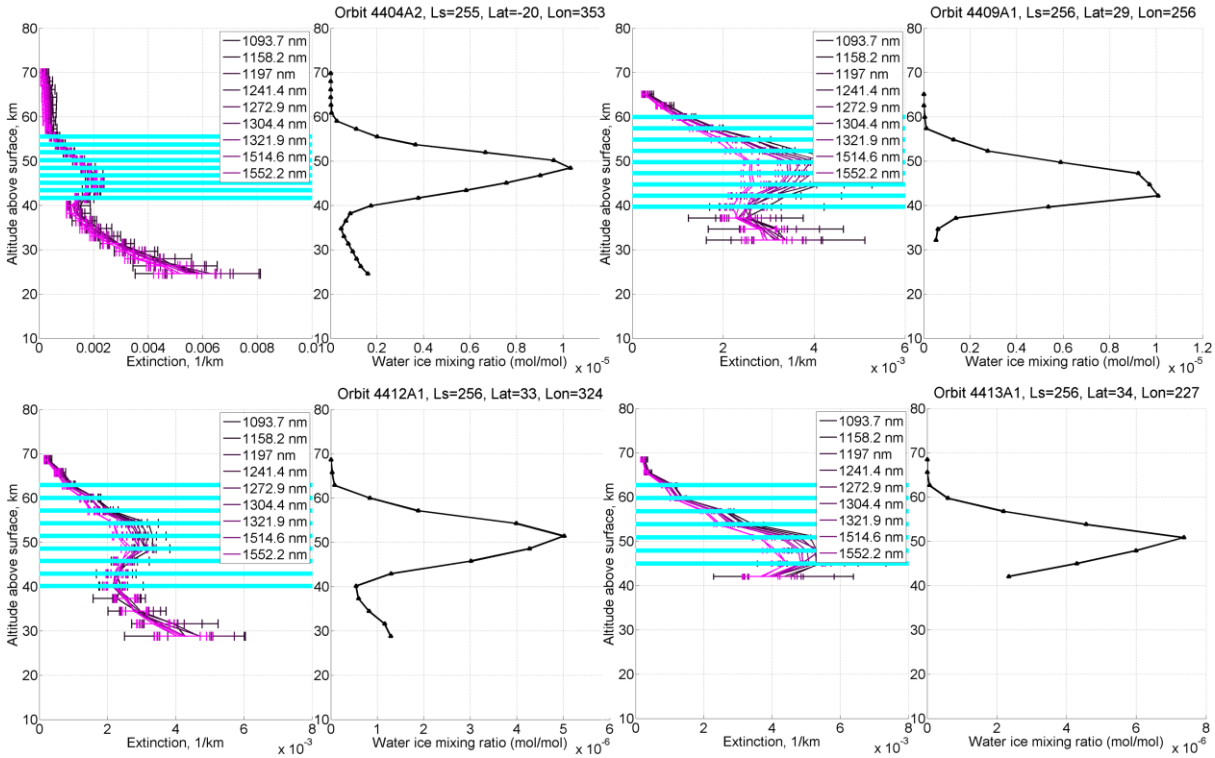

Fig. 3. Examples of orbits with possible ice clouds.

tudes, we should choose the best case of fitting from different effective variances. In previous works this value commonly assumed 0.2 or 0.25. We have selected υ_{eff} based on information about χ^2 (criteria of fitting).

Combining these results we have got information about extinction, particle size, effective variance, number density, the presence of ice clouds and study the distribution and evolution of these values during development of the dust storm.

Results:

Extinction.

Set of profiles was divided on 5 series associated with different latitude bands. The statistics is better for middle latitudes in both hemispheres (Fig.2). It is clear that extinction increases there, or in other terms, significant level of extinction achieves on higher altitudes at the end of the season.

Ice clouds.

Looking for some profiles of extinction we can see the feature that may be described as a local increasing of extinction at selected altitudes. It may indicate a cloud – most likely, cloud of water ice. The additional reasons would be prediction of the model (MCD). Fig.3 demonstrates several examples of the cases where we expect clouds with good agreement with the model.

Effective variance.

As we know lognormal distribution is described by the following:

$$n(r) = Const \cdot r^{-1} \exp\left(-\frac{(\ln r - \ln r_g)^2}{2\ln^2 \sigma_g}\right),$$

where r_g and σ_g are connected with the effective radius and variance as

$$r_{eff} = r_g \exp\left(\frac{5}{2}\ln^2 \sigma_g\right), \quad \upsilon_{eff} = \exp\left(\ln^2 \sigma_g\right) - 1.$$

So if we know the extinction coefficient at an altitude z for several wavelengths λ we can constrain the size distribution of the refracting particles at that altitude solving the inverse problem:

$$k_{ext}(\lambda, z) = \int_0^\infty \sigma_{ext}(\lambda, r) n(r, z) dr \ , \text{ where}$$

$$\sigma_{ext}(\lambda, r) = Q_{ext}(r, m, \lambda)\pi r^2 ,$$

and Q_{ext} is the extinction cross-section factor and may be calculated by Mie theory for corresponding refractive index m, wavelength λ and a given size distribution.

After this procedure we should choose the best from 5 cases with different variance υ_{eff} from 0.1 to 0.5 (suppose we know that there are no clouds in that point). This also manual work was done based on the information about χ^2, behavior of the fitting function and corresponding values of effective radius, because in some cases the solving algorithm didn't converge. Often it was difficult to select automatically because of uncertainties of input extinction data.

Particle size.

Size distribution of the aerosol particles was reconstructed by the way described above. After the best fit was found it allows to compare corresponding radiuses at different time and coordinates. Special interest concerns with high altitude dust loading and transport processes during the storm event.

So we binned our data into 6 altitude bands: below 30 km, 30-40 km, 40-50 km, 50-60 km, 60-70 km and above 70 km. For each band the evolution of effective radius value is presented on Fig.4, where the color corresponds to latitude in Northern and southern hemispheres.

Some trends may be noticed. For example, we see certain increasing of radius in altitude range of 50-80 km – at high and middle latitudes of northern hemisphere and at all latitudes of southern.

Number density

We can also look at the same evolution for number density. This value may be calculated with the retrieved particle size distribution and knowing the extinction coefficient profiles as:

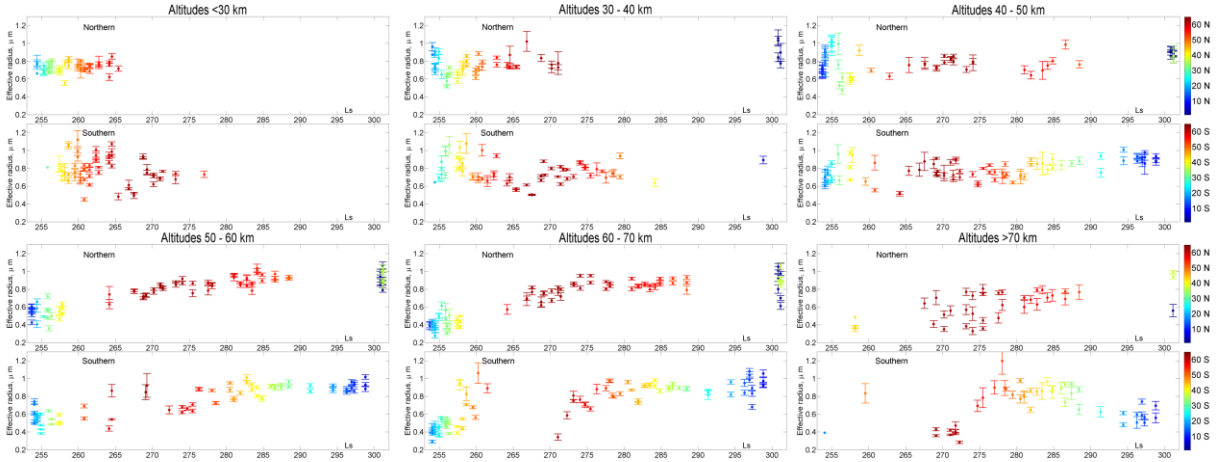

Fig. 4. Evolution of effective radius of dust particles during the global dust storm.

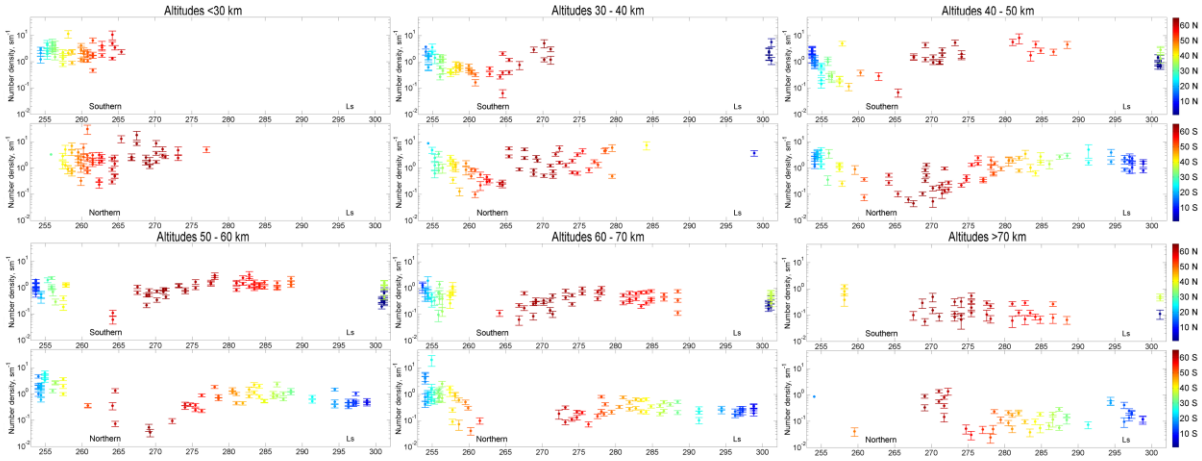

Fig. 5. Evolution of number density of dust particles during the global dust storm.

$$N(z) = \frac{k_{ext}(z)}{\int_0^{\infty} \pi r^2 Q_{ext}(r, m, \lambda) n(r, z) dr}$$

The vertical profiles of density were constrained for 5 cases of v_{eff} values and 10 wavelengths. Then they were averaged by wavelengths, and the best case between 5 fits was chosen according to study described above.

The result is given on the Fig.5. We see the increasing trend at middle latitudes in northern hemisphere at altitudes 60-70 km. At low latitudes there is uncertain trend of decreasing of number density for each latitude range.

Future plans:

Further analysis may be connected with effective radius of water ice particles since these value were calculated by fitting with ice refractive index. This case should be applied to such points where ice clouds were detected. Those results will be compared with models describing processes of water ice clouds' formation.

Also this work will be extended hereafter to other Martian years and seasons.

The work was supported by the RFBR grant 15-02-07812-a and 16-52-16011.

Bibliography:

Fedorova, A.A., Korablev et al. Solar infrared occultation observations by SPICAM experiment on Mars-Express: Simultaneous measurements of the vertical distributions of H2O, CO2 and aerosol. Icarus 200 (March 2009), 96–117.

Fedorova A.A., Montmessin F et al. Evidence for a bimodal size distribution for the suspended aerosol particles on Mars. Icarus 231, March 2014, 239-260.

Korablev, O. et al., 2006. SPICAM IR acousto-optic spectrometer experiment on Mars Express. J. Geophys. Res. 111, E09S03.

Mishchenko, M.I., Dlugach, J.M., Yanovitskij, E.G., Zakharova, N.T., 1999. Bidirectional reflectance of flat, optically thick particulate laters: And efficient radiative transfer solution and applications to snow and soil surfaces. J. Quant. Spectrosc. Radiat. Transf. 63, 409–432.

Montabone L. et al. Eight-year climatology of dust optical depth on Mars. Icarus 251, 65-95, 2015.

Montmessin, F., Rannou, P., Cabane, M., 2002. New insights into martian dust distribution and water-ice cloud microphysics. J. Geophys. Res. 107 (E6).

Warren, S.G., 1984. Optical constants of ice from the ultraviolet to the microwave. Appl. Opt. 23, 1206–1225.

Wolff, M.J. et al., 2009. Wavelength dependence of dust aerosol single scattering albedo as observed by the Compact Reconnaissance Imaging Spectrometer. J. Geophys. Res. 114, E00D04.